European Journal of Pharmaceutical Sciences 180 (2023) 106332

Contents lists available at ScienceDirect

European Journal of Pharmaceutical Sciences

journal homepage: www.elsevier.com/locate/ejps

In silico design, synthesis and evaluation of a less toxic octinoxate alternative with suitable photoprotection properties

Daniella Zambrano, Diana Millán, James Guevara-Pulido *

INQA Research Group, Química Farmacéutica, Universidad El Bosque, Bogotá D.C, Colombia

A R T I C L E I N F O

Keywords:
Ligand based virtual screening
Molar absorptivity
Artificial neural network

A B S T R A C T

Excessive UV exposure leads to several skin pathologies such as sunburns, photoaging and carcinogenesis. Currently, sunscreen use is the most important factor in protecting skin from photoinduced damage. Octinoxate is a commonly used UV filter, but its use has become controversial because it acts as an endocrine disruptor in both humans, and marine animals. Research has relied on biotechnology, structure activity relationship (SAR) studies and combinatorial chemistry to find new and less toxic UV filters. However, there are no current examples that describe the possible applications of *in silico* techniques for obtaining these compounds. Thus, this project sought to design an octinoxate analog that could be used as a less toxic, but equally effective, photoprotective alternative through ligand based virtual screening (LBVS). We designed 213 novel molecules based on the *(E)*-cinnamoyl moiety of octinoxate, but only 23 were found to be less toxic than the parent compound. Then, an artificial neural network (ANN) based model was built to predict the molar absorptivity of those 23 molecules, and the molecule that presented a similar molar absorptivity to that of octinoxate was chosen for synthesis (analog 4, 3-phenylpropyl (*E*)-3-(4-methoxyphenyl)acrylate).

Synthesis for analog 4 resulted in a 90% yield, and its photoprotective properties, lipophilicity and cytotoxicity were then evaluated. Analog 4 absorbed UV radiation in the range of 250–340 nm, and it presented a molar absorptivity of 36,155 $M^{-1}cm^{-1}$. Its lipophilicity was evaluated with RP-HPLC resulting in a $\log_{kw}$ of 2.49 and its LC_{50} was greater than octinoxate's (67.41 nM vs. 45.67 nM). Therefore, results showed that ligand based virtual screening is an effective strategy for the development of new organic UV filters, because it guided the design of less toxic analogs and pinpointed the most likely analog to exhibit UV properties similar to those of octinoxate. In this case, analog 4 is a promising alternative to its parent compound since it proved to be more effective and less toxic.

1. Introduction

Sunscreens are pharmaceutical products designed to help protect the skin against damage caused by UV radiation, such as sunburns, skin cancer and photoaging (Flavia et al., 2022). These products are made of UV filters that can be classified into two main categories: inorganic filters (e.g. zinc oxide, titanium dioxide) reflect the sun's UV radiation, while organic filters absorb it (e.g. cinnamates, salicylates) (Ruszkiewicz et al., 2017).

Octinoxate is a cinnamate derivative commonly used as a UVB filter in sunscreens and a variety of personal care products. However, recent studies have shown that this compound is an endocrine disruptor in both humans and animals, and that it directly contributes to coral bleaching (Gunia-Krzyzak et al., 2018; Siller et al., 2018). Currently, its use has been restricted in coastal areas around the world such as Hawaii, Florida, Indonesia among others, due to its detrimental effect on coral reefs since these ecosystems are worth between 30 and 375 billion USD (Raffa et al., 2019). Additionally, these restrictions directly compromise the pharmaceutical industry since products with octinoxate are highly lucrative (Ridder, 2020a; Ridder, 2020b). Therefore, it has become important to search for less harmful UV filters that also offer similar photoprotection properties as those on the market, in order to replace these harmful molecules without compromising client's adherence to sunscreen products (Levine, 2020).

Current research has relied on expensive and time-consuming strategies namely biotechnology, SAR studies and combinatorial chemistry to search for new UV filters (Padinka, 2018; Promkatkaew et al., 2014; Popiól et al., 2021). Thus, this project sought to explore the possibility

* Corresponding author at: Química Farmacéutica, Universidad El Bosque, Bogotá, Colombia.
E-mail address: joguevara@unbosque.edu.co (J. Guevara-Pulido).

https://doi.org/10.1016/j.ejps.2022.106332
Received 5 July 2022; Received in revised form 12 November 2022; Accepted 14 November 2022
Available online 16 November 2022
0928-0987/© 2022 The Authors. Published by Elsevier B.V. This is an open access article under the CC BY license (http://creativecommons.org/licenses/by/4.0/).

that ligand-based virtual screening can provide a cost-effective alternative strategy for the discovery of these molecules. In this case, ligand based virtual screening was first used to design a series of less ecotoxic octinoxate analogs, and then used to select the analog with the greatest chance to exhibit suitable photoprotective properties. Afterward, the best candidate was synthesized, and its physicochemical and cytotoxic properties were evaluated in order to study the effect of the structural modification on the performance of the analog as a promising UV filter.

2. Materials and methods

2.1. Development of octinoxate analogs

First, octinoxate analogs were designed using the LAZAR Toxicity Predictions software (Maunz et al., 2013) which allowed the characterization of the analogs' toxicity profile via Ligand-Base Virtual Screening (LBVS) using a regression type model to predict acute toxicity (LC_{50}) in *Daphnia Magna* (training set = 546 compounds, max R^2 = 0.785) and *Fathead Minnow* (training set = 580 compounds, max R^2 = 0.506), and a classification type model to predict carcinogenicity in mouse (training set = 980 compounds, max R^2 = 0.782). This allowed the identification of those analogs with a safer toxicity profile than octinoxate.

Then, in order to choose which analogs to synthesize, a suitable training set (commercial UV filters with an *(E)*-cinnamoyl moiety) was first selected from the literature. Next, the structures of the training set and the analogs were optimized in Avogadro employing the *MMFF94s* forcefield and the *Steepest Descent* algorithm with *four steps per update* (Avogadro, 2018). Afterwards, the PaDEL software was used to calculate 52 molecular descriptors associated with the absorption capabilities of these molecules (Yap, 2011).

Then, the correlation between the molecular descriptors and molar absorptivities of the training set was explored using the INQA artificial neural network (Guevara-Pulido et al., 2022). The prediction of the molar absorptivities of the analogs with safer toxicity profiles was performed after carrying out a systematic analysis to identify the number of nodes and the number of molecular descriptors that resulted in the best R^2 value, the closest to 1. Analogs that exhibited a safer toxicity profile than octinoxate, and a similar molar absorptivity value (calculated with an ANN-based prediction model) were the most promising candidates for synthesis.

Table 1
Toxicity profile of the most promising candidates and octinoxate according to LAZAR Toxicity Predictions (Maunz et al., 2013).

Candidate	Structure	LC_{50} *D. magna*	LC_{50} *F. minnow*	Carcinogenicity in mice
Octinoxate		0.007 mM	0.143 mM	Positive
1		0.110 mM	0.325 mM	Negative
2		0.011 mM	0.185 mM	Negative
3		0.011 mM	0.605 mM	Negative
4		0.011 mM	0.440 mM	Negative
5		0.007 mM	0.397 mM	Negative
6		0.256 mM	0.233 mM	Negative
7		0.019 mM	0.270 mM	Negative
8		0.048 mM	0.303 mM	Negative
9		0.047 mM	0.305 mM	Negative
10		0.014 mM	0.317 mM	Negative
11		0.012 mM	0.245 mM	Negative
12		0.027 mM	0.257 mM	Negative
13		0.043 mM	0.433 mM	Negative
14		0.010 mM	0.308 mM	Negative
15		0.256 mM	0.327 mM	Negative
16		0.007 mM	0.511 mM	Negative
17		0.028 mM	0.540 mM	Negative
18		0.013 mM	0.388 mM	Negative
19		0.012 mM	0.453 mM	Negative
20		0.014 mM	0.321 mM	Negative

2.1.1. Synthesis of most promising analogs

Synthesis was accomplished using 2,2,2-trichloro-1,1-dimethylethyl chloroformate as the carboxylic acid activation agent. Carboxylic acids were activated for 30 min using DCM as the reaction medium, and then the alcohol was added for the subsequent esterification of the acid. Esterification was qualitatively followed by TLC, the purification of the esters was carried out by normal-phase chromatography using hexane and isopropyl alcohol (20:1) as the mobile phase, and characterization of the analogs was done by H^1-NMR (400 MHz) and C^{13}-NMR (100 MHz).

Spectra were recorded in $CDCl_3$ or acetone-d6. Chemical shifts for protons were reported in ppm using tetramethylsilane as internal reference. Carbon chemical shifts were reported in ppm using tetramethylsilane and are referenced to the carbon resonance of the solvent. All NMR spectra were recorded on a 400 MHz Bruker III Ascend Spectrometer equipped with an Advance NEO 400 console and both, BBI and BBO probes. IR spectra were recorded on a FT-IR instrument, while high resolution mass spectra were performed by positive electrospray ionization using a quadrupole-time-of-flight detector (ESI(+)-Q-TOF) instrument. All compounds were purchased from commercial sources and used as received.

2.1.2. Evaluation of the uv properties of the synthesized analog

Spectrophotometric assays were carried out on a Thermo Scientific™ GENESYS™ UV–Vis Spectrophotometer [Detector type: Dual Silicon Photodiodes; Spectral Bandwidth: 1.8 nm; Scan Speed Up to 3600 nm/min; Optical Design: Double Beam-Internal Reference Detector; 50/60 Hz; Photometric Linearity Up to 3.5 Å at 260 nm; Stray Light <0.08%T at 220, 340 nm (NaI, $NaNO_2$) <1.0%T 198–200 nm (KCl); Wavelength Accuracy: ±1 nm; Wavelength Repeatability: ±0.5 nm].

Assays were used for the determination of the molar absorptivity and photostability of the analog. Molar absorptivity was calculated by measuring the absorbance of five solutions of concentration s ranging between 10^{-6}–10^{-5} M. Then, a linear regression was established between the concentration of each solution and its respective absorbance, and through Beer's Law, the molar absorptivity of the analog was determined (Popiól et al., 2021). The photostability of both the analog and octinoxate was evaluated by irradiating a solution of each compound for 60 min at 310 nm (3.40 - 3.45 × 10^{-5} M). The resulting absorbance was compared to the initial one and the percentage of absorbance loss (LoA) was calculated at the λ_{max} (Peyrot et al., 2021). Calculations for estimating LoA were made in triplicate in order to obtain statistically reliable results.

2.1.3. Evaluation of the lipophilicity of the synthesized analog

The lipophilicity of the analog and octinoxate was estimated using RP-HPLC on a Shimadzu HPLC system (Japan, Prominence-i model LC 2030) at 300 nm, with an Ultra Aqueous (AQ) C18 column, according to a previously established methodology (Elmansi et al., 2019). First, the retention times of both molecules were determined at five different proportions of a methanol/water mobile phase (60/40, 65/35, 70/30, 75/25, 80/20 and 90/10). Then, the capacity factor was calculated and a linear relationship between the logarithm of the capacity factor and the percentage of methanol in each mobile phase was established, and the chromatographic index of lipophilicity was derived from the resulting linear equation (y-intercept). Calculations for estimating the chromatographic index of lipophilicity were made in duplicate as shown by Elmansi et al. (2019).

2.1.4. Evaluation of the cytotoxicity of the synthesized analog

The cytotoxicity of the analog was evaluated by applying ISO 10,993–5 test methods (Jiménez et al., 2015). Testing was carried out using fibroblast L929 cells [NCTC clone 929, derivative of Strain L (CCL-1)] purchased from ATCC (Manassas, VA, USA), and Dulbecco's Modified Eagle Medium (DMEM) supplemented with fetal bovine serum (10x), antibiotic-antimycotic solution (10 ×), MEM vitamin solution (10

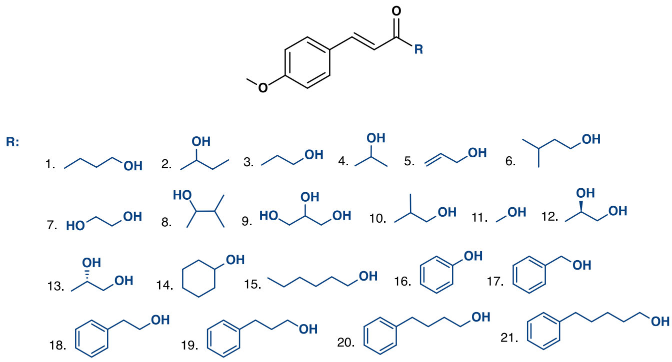

Fig. 1. Aromatic and aliphatic alcohols used to modify the ester moiety of octinoxate for the first set of analogs.

×) and sodium pyruvate solution (10 ×) (Thermo Fisher Scientific, Waltham, MA, USA).

First, cells were seeded into 96-well plates (1 × 104 cells/100 μL medium) and incubated (37 °C, 5% CO_2) for 24 h in supplemented DMEM. Afterward, the culture medium was replaced by different concentrations of the analog (0–150 nM) and cells were incubated again for 24 h under the same conditions. Sterile DMEM supplemented with DMSO (25% v/v) and DMEM incubated with silicone (0.2 g/mL) were used as positive and negative controls, respectively. Then, the medium was removed and 100 μL of MTT (3-(4,5-Dime- thylthiazol-2-yl)−2,5-Diphenyltetrazolium Bromide) (1 mg/mL) was added, and samples were incubated for 2 h (37 °C, 5% CO_2). After discarding the MTT, DMSO (100 μL) was added to dissolve the formazan crystals, and the cell viability percentage was determined by UV/VIS spectrophotometry at 570 nm (Bio-Rad, xMARK). LC_{50} values were then estimated by establishing a linear regression between the analog concentrations and the cell viability percentage. Calculations were made in triplicate in order to obtain statistically reliable results.

3. Results and discussion

The toxicity profile of octinoxate according to LAZAR Toxicity Predictions (Maunz et al., 2013) was determined as an initial step, which can be observed in Table 1. From these results, only the analogs that exhibited LC_{50} values greater than octinoxate's in both *Daphnia magna* and *Fathead minnow*, as well as negative carcinogenicity in mice would be considered promising candidates. In this case, both *D. magna* and *F. minnow* act as indicator species to assess the response of aquatic ecosystems to pollutants. Their response to common pollutants measures how detrimental a pollutant can be to aquatic species and ecosystems.

The first set of analogs consisted in modifying the ester moiety of octinoxate with several aromatic and aliphatic alcohols, as shown in Fig. 1. The toxicity profile of the most promising candidates of this set is presented in Table 1.

According to the structure of the most promising candidates from this set (Table 1, entries 2–6) the best ester is aromatic with a maximum four-carbon chain. Now, this was beneficial because by increasing the number of chromophore groups in the analogs' structure the amount of UV radiation that they would absorb would most likely increase as well (Popiól et al., 2021), therefore resulting in more efficacious UV filters.

Afterwards, for the second set of analogs, the most promising candidates of the first set were modified as shown in Fig. 2. This set didn't yield promising candidates which indicated that the cinnamate ring must be substituted, but with a less reactive functional group such as an ether.

Therefore, for the third set of analogs the methoxy group of the original molecule was modified with ethoxy and propoxy (Fig. 3) and the best position for this substitution on the cinnamate ring was also determined. Only the *ortho* and *para* positions were evaluated because the cinnamate chain is an *ortho/para* directing group; consequently, rendering the *meta* position inactive. The inactivation of this position is relevant in this case because the conjugation would be less than with the *ortho* and *para* positions and maximizing this conjugation could lead to the analogs presenting bathochromic and hyperchromic shifts and a greater molar absorptivity (Peyrot et al., 2021), both of which would increase the efficacy of the analogs as UV filters.

The most promising candidates of this set are shown in (Table 1 entries 7–8), and their structure made it possible to conclude that the best ether for the cinnamate ring is methoxy and that aside from the *para* position, the *ortho* position also contributes to decrease the toxicity of the analogs.

Then, the fourth set of analogs sought to evaluate the effect of adding a substitution to the ester ring of the most promising candidates of the previous sets, and its most favorable position on that ring (Fig. 4). This set yielded several promising candidates (Table 1, entries 9–21), from

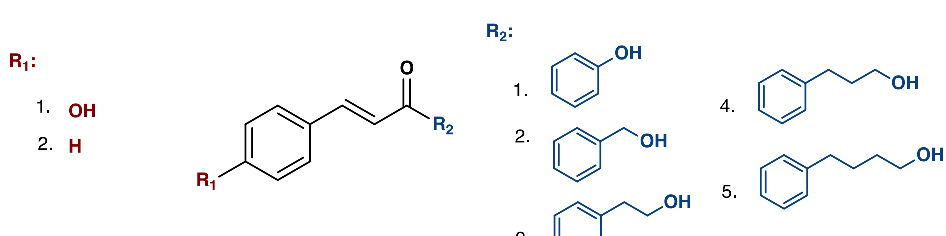

Fig. 2. Functional groups used to modify the substitution of the cinnamate ring of octinoxate for the second set of analogs.

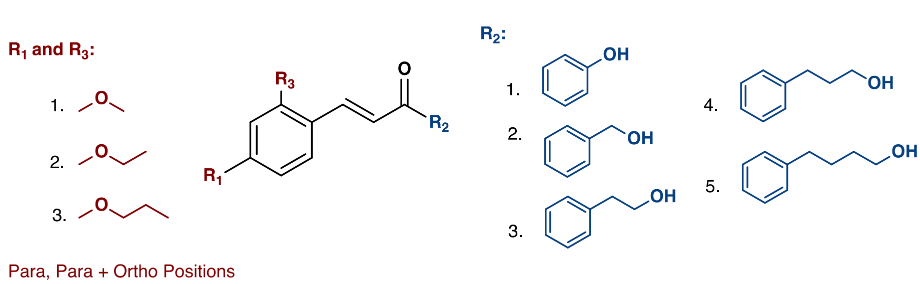

Fig. 3. Functional groups used to modify the substitution of the cinnamate ring of octinoxate for the third set of analogs.

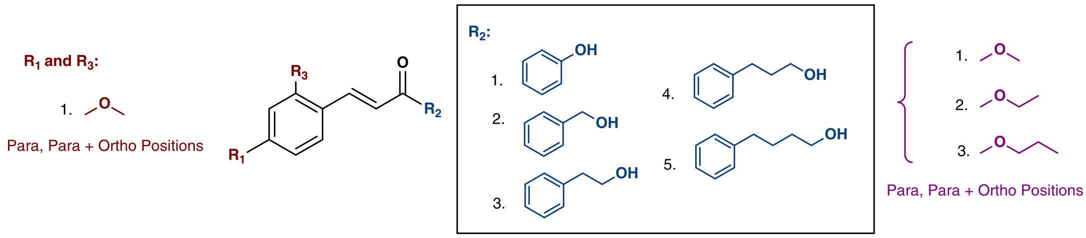

Fig. 4. Structural modifications of the fourth set.

Table 2
Toxicity profile of the most promising candidates of the fifth set.

Candidate	Structure	LC_{50} *D. magna*	LC_{50} *F. minnow*	Carcinogenicity in mice
21		0.062 mM	0.322 mM	Negative
22		0.014 mM	0.259 mM	Negative
23		0.007 mM	0.359 mM	Negative

Table 3
Predicted molar absorptivities of the octinoxate analogs.

Entry	UV Filters	Predicted ε ($M^{-1}cm^{-1}$)
1	phenyl (*E*)−3-(4-methoxyphenyl)acrylate	19,862
2	benzyl (*E*)−3-(4-methoxyphenyl)acrylate	20,195
3	phenethyl (*E*)−3-(4-methoxyphenyl)acrylate	21,643
4	3-phenylpropyl (*E*)−3-(4-methoxyphenyl)acrylate	22,354
5	4-phenylbutyl (*E*)−3-(4-methoxyphenyl)acrylate	22,830
6	phenethyl (*E*)−3-(2-methoxyphenyl)acrylate	19,816
7	4-phenylbutyl (*E*)−3-(2,4-dimethoxyphenyl) acrylate	22,742
8	2-methoxyphenyl (*E*)−3-(4-methoxyphenyl) acrylate	19,673
9	2,6-dimethoxyphenyl (*E*)−3-(4-methoxyphenyl) acrylate	19,487
10	2,6-diethoxyphenyl (*E*)−3-(4-methoxyphenyl) acrylate	19,348
11	2-ethoxyphenyl (*E*)−3-(4-methoxyphenyl)acrylate	19,787
12	2-methoxybenzyl (*E*)−3-(4-methoxyphenyl)acrylate	20,024
13	2,6-dimethoxybenzyl (*E*)−3-(4-methoxyphenyl) acrylate	19,847
14	2,6-diethoxybenzyl (*E*)−3-(4-methoxyphenyl) acrylate	20,973
15	2,6-dimethoxyphenethyl (*E*)−3-(2-methoxyphenyl) acrylate	19,446
16	2-methoxyphenethyl (*E*)−3-(4-methoxyphenyl) acrylate	21,513
17	2,6-dimethoxyphenethyl (*E*)−3-(4-methoxyphenyl) acrylate	21,377
18	2,6-diethoxyphenethyl (*E*)−3-(4-methoxyphenyl) acrylate	21,263
19	3-(2,6-dimethoxyphenyl)propyl (*E*)−3-(4-methoxyphenyl)acrylate	22,137
20	3-(2,6-diethoxyphenyl)propyl (*E*)−3-(4-methoxyphenyl)acrylate	22,810
21	2,6-dimethoxyphenyl (*E*)−3-(4-methoxyphenyl) but-2-enoate	16,862
22	2-methoxyphenyl (*E*)−3-(4-methoxyphenyl)but-2-enoate	17,086
23	4-phenylbutyl (*E*)−3-(4-methoxyphenyl)−3-phenylacrylate	22,283

which it can be concluded that the best substitutions for the ester ring were the methoxy and ethoxy groups in the *ortho* position of the ring.

Lastly, the photodegradation products of octinoxate were examined in order to evaluate the compounds that would probably result from the photodegradation of the candidates obtained from the previous four sets. According to Stein et al. (2017), 4-methoxybenzaldehyde is a common product of the photodegradation of octinoxate. This compound is very reactive; thus, three functional groups (methyl, ethyl, and phenyl) were added to the alkene group of the candidates in order to avoid the formation of this subproduct via hyperconjugation and thus, avoid its possible contribution to the toxicity profile of the analogs. The best candidates of this set are presented in Table 2.

Now, in order to test the absorption capabilities of the 23 most promising candidates, we set out to build a prediction model using an artificial neural network (ANN) that enabled the prediction of the molar absorptivity of the analogs. The model was built as described in the methodology, which allowed after a systematic analysis the selection of eight molecular descriptors (AlogP, PetitjeanNumber, $nsCH_3$, nAtomLC, nAtomLAC, TopoRadius, TopoDiameter y nHBd). These descriptors, the experimental molar absorptivity values of the training set (Graph 1, A-O) and 640 hidden nodes yielded a determination coefficient (R^2) of 0.768, enabling the prediction of the molar absorptivity of the analogs (Table 3, entries 1–23).

(A)-(E)−3-phenyl-1-(12,32,52,72-tetrapropoxy-1,3,5,7(1,3)-tetra-benzenacyclooctaphane-15-yl)prop-2-en-1-one[45], (B)-(Z)−1-(55-cinnamoyl-12,32,52,72-tetrapropoxy-1,3,5,7(1,3)-tetrabenzenacyclooctaphane-15 yl)−3-phenylprop-2-en-1-one [45], (C)-isopentyl (E)−3-(4-methoxyphenyl)acrylate [46], (D)-(E)−3-(4-hydroxy-3-methoxyphenyl)acrylic acid [47], (E)-(E)−3-(4-(((Z)−3,7-dimethylocta-2,6-dien-1-yl)oxy)−3-methoxyphenyl)acrylic acid [47], (F)−2-ethoxyethyl (E)−3-(4-methoxyphenyl)acrylate [46, (G)−2-ethylhexyl 2-cyano-3,3-diphenylacrylate [46], (H)-(E)−3-(4-methoxyphenyl)acrylate[46], (I)−2-ethylhexyl-(Z)−3-(4-methoxyphenyl)acrylate-2-ethylhexyl[48], (J)-(E)−3-(2,4,5-trimethoxyphenyl)acrylate [48], (K)−2-ethylhexyl-(E)−3-(4-methoxyphenyl)acrylate (Octinoxate) [47], (L)-(E)−3-(3-methoxy-4-((3-methylbut-2-en-1-yl)oxy)phenyl) acrylic acid, [47] (M)−2-ethylhexyl (E)−3-(3-methoxyphenyl)acrylate [47], (N)−2-ethylhexyl (E)−3-(2,4,6-trimethoxyphenyl)acrylate [47], (O)−2-ethylhexyl (E)−3-(2-methoxyphenyl)acrylate[47].

Based on the results shown in (Table 3, Fig. 5) entries 4, 5, 7, 19, 20 and 23 presented molar absorptivity values closer than the value reported for octinoxate (Table 3, entry K, Fig. 5). However, analogs 5 and 23 were dismissed because their LC_{50} values in *Daphnia Magna* (0.007 nM, Tables 2 and 5) were significantly lower than those of the other four entries. On the other hand, entries 5, 8, 20 and 21 had similar toxicity profiles (Table 1), but only candidates 4 and 7 were chosen for synthesis.

Candidates 4 and 7 were obtained according to Schemes 1 and 2, respectively, using 2,2,2-trichloro-1,1-dimethylethyl chloroformate to generate the mixed anhydride derivative of each carboxylic acid. Since methoxy-substituted cinnamic acids are not highly reactive, the reaction is favored by the "proton sponge" effect of triethylamine in dichloromethane (DCM) at room temperature, thus allowing the in-situ preparation of the mixed anhydrides which are then made to react with their respective alcohol (10% excess) under soft reaction conditions at room temperature. Also, this methodology favors the addition-elimination step via which each ester is formed under soft conditions and with high percent yields. However, synthesis of candidate 4 resulted in a greater percent yield than synthesis of candidate 7, probably due to the fact that the additional substitution on the cinnamate ring of candidate 7 decreases the partial positive charge on its carboxyl carbon, thus reducing the effectiveness of the nucleophilic attack by the alcohol. As a

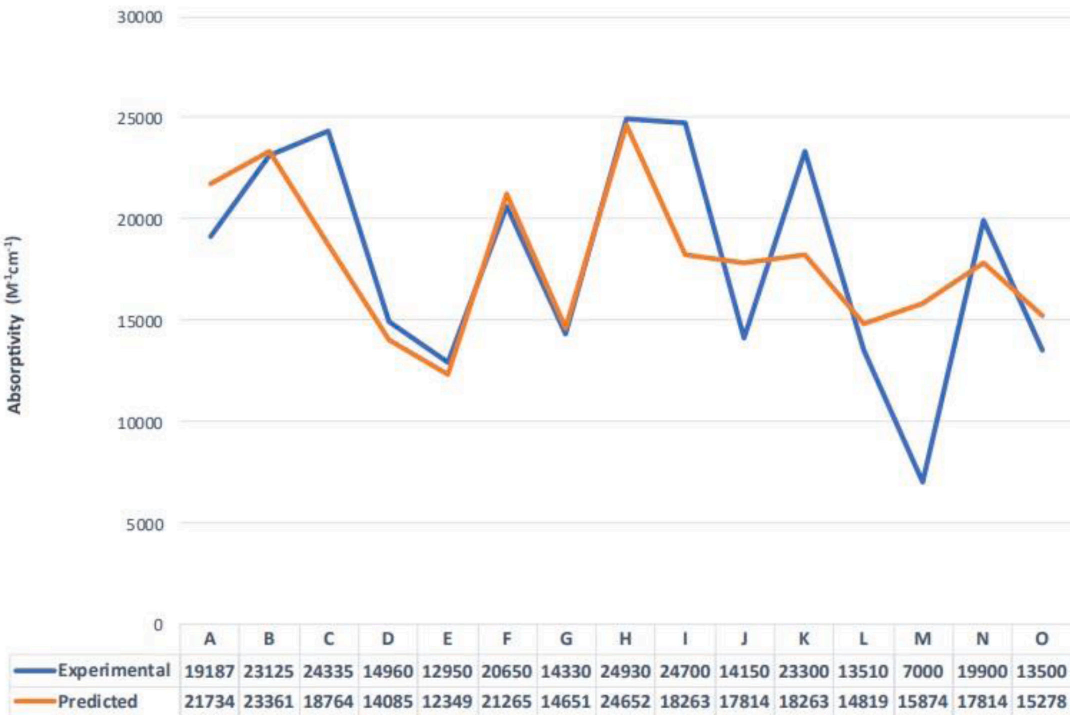

	A	B	C	D	E	F	G	H	I	J	K	L	M	N	O
Experimental	19187	23125	24335	14960	12950	20650	14330	24930	24700	14150	23300	13510	7000	19900	13500
Predicted	21734	23361	18764	14085	12349	21265	14651	24652	18263	17814	18263	14819	15874	17814	15278

Fig. 5. Experimental and predicted molar absorptivities of the training set. (For interpretation of the references to colour in this figure legend, the reader is referred to the web version of this article.).

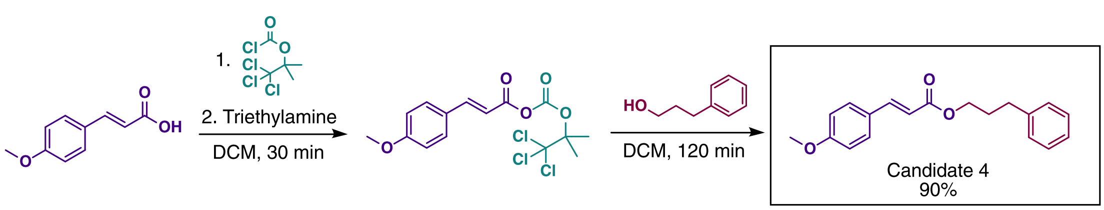

Scheme 1. Synthesis of 3-phenylpropyl (*E*)−3-(4-methoxyphenyl)acrylate (Analog 4).

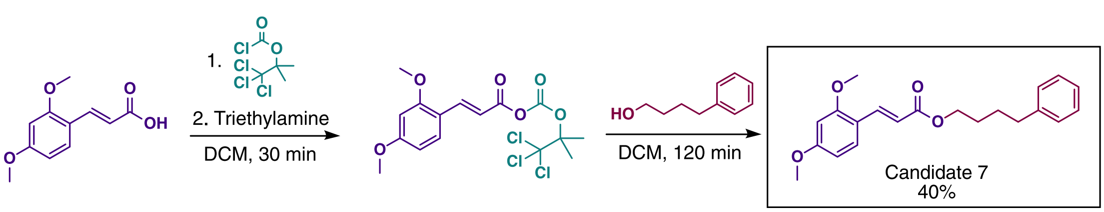

Scheme 2. Synthesis of 4-phenylbutyl (*E*)−3-(2,4-dimethoxyphenyl)acrylate (Analog 7).

result, only the UV properties, lipophilicity, and cytotoxicity of candidate 4 were determined.

Once candidate 4 was characterized, its UV properties were evaluated spectrophotometrically. According to Fig. 6, candidate 4 presented absorbance mostly at UVB wavelengths (280–315 nm), which led to a wavelength coverage area comparable to that of octinoxate.

Afterwards, the molar absorptivity and loss of absorbance of candidate 4 were determined. As shown in Table 4, candidate 4 presented a greater molar absorptivity than the one reported in the literature for octinoxate. This indicates that candidate 4 has the ability to absorb more radiation than octinoxate at the same UVB wavelengths (Skoog et al., 2014), thus, being capable of offering greater photoprotection.

Furthermore, it can be observed that the experimental value is significantly larger than the one predicted by the neural network model. This can be attributable to the fact that the prediction was carried out with an R^2 value of 0.768, because even though this value is capable of offering reliable predictions (Carpenter et al., 2018), also has a wider margin of error than if the prediction had been carried out with an R^2 value closer to 1.0. Nevertheless, the experimental results of this variable proved that the prediction model was able to guide the selection of less toxic analogs towards the one that had the greatest possibility to exhibit a molar absorptivity value similar to that of octinoxate.

On the other hand, Table 4 also shows that the loss of absorbance of both candidate 4 and octinoxate is similar since their respective confidence intervals overlap. Considering that the loss of absorbance is related to the photostability of these molecules upon UV radiation, these results indicate that both candidate 4 and octinoxate will preserve their protective effect for a similar amount of time, which might also suggest that the frequency of their application would be similar as well.

Now, aside from their UV properties, the lipophilicity of promising

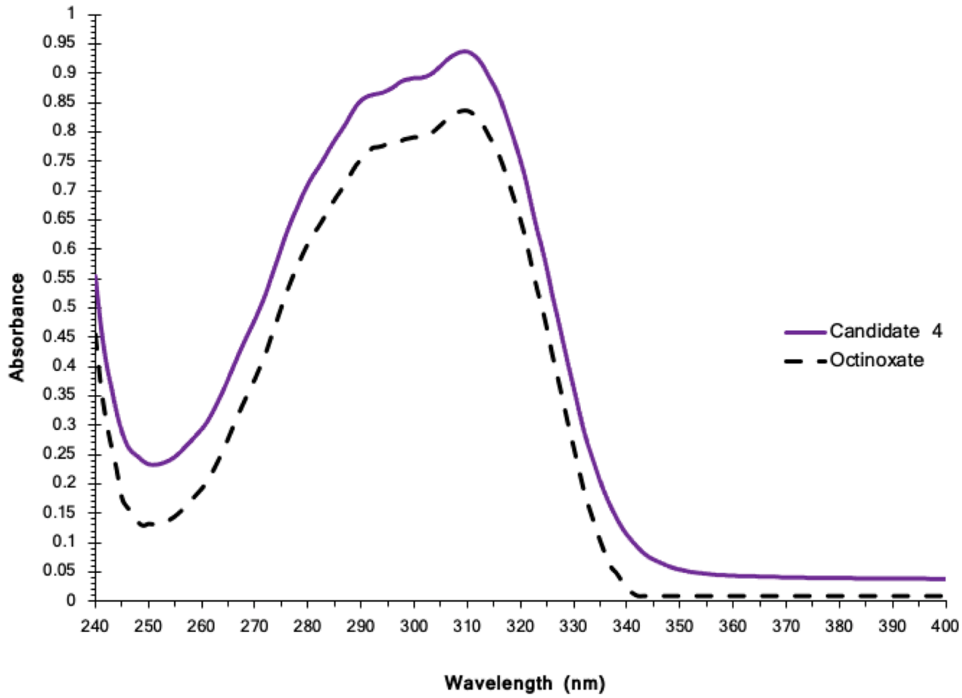

Fig. 6. UV spectra of candidate 4 and octinoxate.

Table 4
Molar absorptivity and loss of absorbance of candidate 4 and octinoxate.

	Molar Absorptivity (M^{-1} cm^{-1})		Loss of Absorbance (%)	Chromatographic Index of Lipophilicity (log*kw*)
Candidate 4	36,155	22,354 (INQA Neural Network)	2.0 ± 1.9 (95% CI 0.1, 3.9)	2.4946
Octinoxate	23,300 [46]		1.0 ± 0.2 (95% CI 0.8, 1.2)	4.2526

UV filters must be evaluated due to the fact that the functionality of these molecules depends on their ability to remain on the skin's surface, and the toxic effects often associated with these types of compounds are attributable to their systemic absorption. According to the literature, molecules with lipophilicity values between 1 and 3 will easily permeate the skin because their amphipathic nature allows them to cross the lipophilic barrier of the stratum corneum and the hydrophilic layers of the epidermis (Popiól et al., 2021). Moreover, molecules with lipophilicity values less than −1 will not be able to cross the stratum corneum, whereas those with values greater than 3 will be retained in the stratum corneum, thus delaying their systemic absorption (Popiól et al., 2021).

Thus, Table 4 shows the chromatographic index of lipophilicity of candidate 4 and octinoxate. These results indicate that octinoxate is more lipophilic than candidate 4; yet candidate 4 can permeate the skin

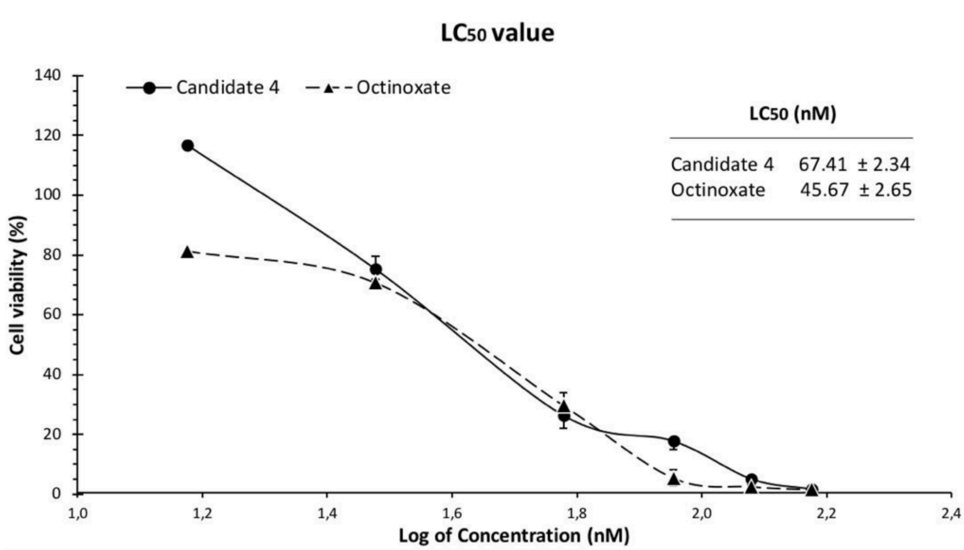

Fig. 7. Effect of candidate 4 and octinoxate on the cell viability of L929 cells.

more easily than octinoxate, thereby making candidate 4 more likely to be absorbed systemically. However, the likelihood of candidate 4 permeating the skin could be reduced by using the appropriate formulation, for example an emulgel. The emulsion moiety of the emulgel would aid the incorporation of candidate 4 into a gel matrix, where it would be trapped and slowly diffuse out into the skin (Supriya et al., 2014). The viscosity of the gel matrix would most likely play a critical role on the amount of time candidate 4 would be retained in the surface of the skin, thus reducing the rate of systemic absorption while also increasing the duration of its protective effects. Nevertheless, more studies – i.e. an in vitro drug release study, are required to determine if modulating the viscosity of an emulgel would significantly reduce skin permeation of this compound.

Finally, the effect of candidate 4 and octinoxate on cell survival was evaluated using L929 cell lines to determine their safety profiles. As shown in Fig. 6, cell viability was reduced as the concentration of both molecules increased.

However, with these results the LC_{50} values of each molecule were determined, which are presented in Fig. 7. These values indicate that candidate 4 is less cytotoxic than octinoxate because a greater amount of it is needed to induce cellular damage or death.

4. Conclusion

Ligand based virtual screening proved to be a useful strategy for designing less ecotoxic octinoxate analogs, and for guiding the selection of these analogs towards the one that could potentially exhibit similar photoprotective properties to those of the parent compound. Synthesis of the most promising analog was supported by H^1-NMR and C^{13}-NMR spectra, and the physicochemical and biological assays performed showed that the analog presented a greater molar absorptivity than octinoxate (36,155 $M^{-1}cm^{-1}$ vs. 23,300 $M^{-1}cm^{-1}$) and a similar absorbance loss (2.0% vs. 1.0%). Thus, the analog can be considered a more effective alternative to octinoxate. On the other hand, the analog exhibited a greater LC_{50} than octinoxate (67.41 nM vs. 45.67 nM), which indicates that the analog can also be considered a less cytotoxic substitute to its parent compound.

CRediT authorship contribution statement

Daniella Zambrano: Conceptualization, Methodology, Software, Data curation, Writing – original draft, Investigation, Software, Validation. **Diana Millán:** Methodology, Visualization. **James Guevara-Pulido:** Conceptualization, Methodology, Software, Data curation, Writing – original draft, Investigation, Writing – review & editing, Supervision.

Data availability

Data will be made available on request.

Acknowledgement(s)

This project was funded by INQA Research Group associated to the Pharmaceutical Chemistry Program at Universidad El Bosque, Bogotá Colombia.

References

Avogadro. Molecular Mechanics and Force Field. Avogadro, 2018. Obtenido de: https://avogadro.cc/docs/optimizing-geometry/molecular-mechanics.

Carpenter, K.A., Cohen, D.S., Jarrell, J.T., 2018. Huang X. Deep learning, and virtual drug screening. Future Med. Chem. 10 (21), 2557–2567. https://avogadro.cc/docs/optimizing-geometry/molecular-mechanics/.

Elmansi, H., Nasr, J.J., Rageh, A.H., El-Awady, M.I., Hassan, G.S., Abdel-Aziz, H.A., Belal, F., 2019. Assessment of lipophilicity of newly synthesized celecoxib analogues using reversed-phase HPLC. BMC Chem. 13 (1) https://doi.org/10.1186/s13065-019-0607-6.

Flavia, A., Baptista, C., Gomes, E.E., Lupi, O., Reato, C., Amante, H., 2022. Sunscreen lotions in the dermatological prescription: review of concepts and controversies. An Bras de Dermatol 97 (2), 204–222. https://doi.org/10.1016/j.abd.2021.05.012.

Guevara-Pulido, J., Jimenez, R.A., Morantes, S.J., Jaramillo, D.N., 2022. Acosta-Guzman P. Design, Synthesis, and Development of 4-[(7-C*hloroquinoline*-4-*yl*)*amino*]phenol as a Potential SARS-CoV-2 Mpro Inhibitor. Chem. Select 7 (15). https://doi.org/10.1002/slct.202200125.

Gunia-Krzyzak, A., Sloczynska, K., Popiól, J., Koczurkiewicz, P., Marona, H., Pekala, E., 2018. Cinnamic acid derivatives in cosmetics: current use and future prospects. Int. J. Cosmetic. Sci. 40 (4), 356–366. https://doi.org/10.1111/ics.12471.

Jiménez, R.A., Millán, D., Suesca, E., Sosnik, A., Fontanilla, M.R, 2015. Controlled release of an extract of Calendula officinalis flowers from a system based on the incorporation of gelatin-collagen microparticles into collagen I scaffolds, design and in vitro performance. Drug Deliv. Transl. Res. 5 (3), 209–218. https://doi.org/10.1007/s13346-015-0217-3.

Levine, A., 2020. Sunscreen use and awareness of chemical toxicity among beach goers in Hawaii prior to a ban on the sale of sunscreens containing ingredients found to be toxic to coral reef ecosystems. Mar. Policy. https://doi.org/10.1016/j.marpol.2020.103875.

Maunz, A., Gutlein, M., Rautenberg, M., Vorgrimmler, D., Gebele, D., Helma, C, 2013. Lazar: a modular predictive toxicology framework. Front. Pharmacol. 4 https://doi.org/10.3389/fphar.2013.00038.

Padinka, M., 2018. Looking to nature for new sunscreens. ACS Cent. Sci. 4, 788–790. https://doi.org/10.1021/acscentsci.8b00433.

Peyrot, C., Mention, M.M., Brunissen, F., Allais, F., 2021. Sinapic acid esters: octinoxate substitutes combining suitable UV protection and antioxidant activity. Antioxidants 9 (9), 782. https://doi.org/10.3390/antiox9090782.

Popiól, J., Gunia-Krzyzak, A., Sloczynska, K., Koczurkiewicz-Adamczyk, P., Piska, K., Wojcik-Pszczola, K., Zelaszczyk, D., Krupa, A., Zmudzki, P., Marona, H., Pekala, E, 2021. The involvement of xanthone and (E)-cinnamoyl chromophores for the design and synthesis of novel sunscreening agents. Int. J. Mol. Sci. 22 (1), 34. https://doi.org/10.3390/ijms22010034.

Promkatkaew, M., Suramitr, S., Karpkird, T., Wanichwecharungruang, S., Ehara, M., Hannongbua, S., 2014. Photophysical properties and photochemistry of substituted cinnamates and cinnamic acids for UVB blocking: effect of hydroxy, nitro, and fluoro substitutions at ortho, meta, and para positions. Photochem. Photobiol. Sci. 13 (3), 583. https://doi.org/10.1039/c3pp50319d.

Raffa, R.B., Pergolizzi, J.V., Taylor, R., Kitzen, J.M., 2019. Sunscreen bans: coral reefs and skin cancer. J. Clin. Pharm. Ther. 44 (1), 134–139. https://doi.org/10.1111/jcpt.12778.

Ridder, M., 2020a. Leading suntan lotion and oil brands in the U.S. sales 2019. Statista. Obtenido de. https://www.statista.com/statistics/301160/suntan-lotion-and-oil-brands-sales-in-the-us/.

Ridder, M., 2020b. Dollar sales of the leading lip balm/treatment brands in the United States in 2019. Statista. Obtenido de. https://www.statista.com/statistics/463359/us-sales-of-leading-lip-balm-treatment-brands/.

Ruszkiewicz, J.A., Pinkas, A., Ferrera, B., Peresa, T.V., Tsatsakisb, A., Aschne, M., 2017. Neurotoxic effect of active ingredients in sunscreen products, a contemporary review. Toxicol. Rep. 4, 245–259. https://doi.org/10.1016/j.toxrep.2017.05.006.

Siller, A., Blaszak, S., Lazar, M., 2018. Olasz Harken E. Update about the effects of the sunscreen ingredients oxybenzone and octinoxate on humans and the environment. Plast. Surg. Nurs. 38 (4), 158–161. https://doi.org/10.1097/PSN.0000000000000244.

Skoog, D., West, D.M., Holler, F.J., Crouch, S.R., 2014. Deriving Beer's Law. Fundamentals of Analytical Chemistry, 9th Ed. Brooks/Cole Cengage Learning. PDF, pp. 660–663.

Stein, H.A., Berg, C.J., Maung, J.N., O'Connor, L.E., Pagano, A.E., MacManus, L.A., Paulic, S., Paulic, M.G, 2017. Photolysis and cellular toxicities of the organic ultraviolet filter chemical octyl methoxycinnamate and its photoproducts. Environ. Sci. Processes Impacts 19, 851–860. https://doi.org/10.1039/c7em00059f.

Supriya, U., Seema, C., Preeti, K, 2014. Emulgel: a boon for dermatological diseases. IJPRAS 3 (4), 1–9.

Yap, C.W., 2011. PaDEL-descriptor: an open-source software to calculate molecular descriptors and fingerprints. J. Comput. Chem. 32 (7), 1466–1474. https://doi.org/10.1002/jcc.21707.